Chemical and Biomolecular Engineering
2026, Vol. 11, No. 2, pp. 26–34
https://doi.org/10.11648/j.cbe.20261102.12

Research Article

Enhanced Photocatalytic Activity of g-C_3N_4@$Bi_{12}O_{15}X_3$ (X = Br, Cl) Heterostructure Nano-composite

Gashaw Beyene Kassahun*, **Kinde Yeneayehu Teshale**

Applied Physics Department, Adama Science and Technology University, Adama, Ethiopia

Abstract

Bismuth oxyhalides (BiOX, where X = F, Cl, Br, I) are layered and thin film materials with unique physical, chemical, optical as well as structural properties. In this study extensively investigates bismuth oxyhalide based materials photocatalytic application. Due to the layered structure of BiOX based materials used for removal of water pollutant. The removal of pollutant from waste water is a priority duty their toxic properties. Especially, polluted water wasted from dye, textile and leather factories have the properties of carcinogenic and mutagenic. For this purpose the authors synthesized new g-C_3N_4@$Bi_{12}O_{15}X_3$ (X = Cl, Br) nano-composite materials using different synthesize techniques. The synthesized materials are characterized by using different instruments to identify their important and required properties. Their optical, structural, morphology, electronic and photocatalytic response is investigated. The photocatalytic application of this synthesized materials are checked by using water pollutant model dyes (methyl orange (MO) and methylene blue (MB)) and real polluted water by collecting from KK textile industry. They synthesized materials g-C_3N_4@$Bi_{12}O_{15}X_3$ (X = Cl, Br) are very stable and very nice photavcatlitic activity and application. Regarding to photocatalytic application, the photocatalytic response of g-C_3N_4@$Bi_{12}O_{15}Cl_3$ (using MB), g-C_3N_4@$Bi_{12}O_{15}Br_3$ (using MB) and g-C_3N_4@$Bi_{12}O_{15}Cl_3$ (using polluted water) are 97.95%, 96.97% and 96.76%, respectively. In general, the photocatalytic application of bismuth based nanocomposite materials specially g-C_3N_4@$Bi_{12}O_{15}X_3$ (X = Cl, Br, I) have very interested responses.

Keywords

Photo-degradation, Recyclability, Heterostructure, Graphite, Pollutant

1. Introduction

Nowadays, many industries/factories are planting throughout the world even in the developing countries (including Ethiopia). These huge number of factories/industries discharge untreated squander water to the environment. By-products which discharge from dye and textile industries are fragrant compounds, possibly harmful and troublesome to debase. The discharge of squander water from these sites can specifically influence atmosphere, soil, sea-going life forms as well as human and plant wellbeing [1]. Additionally, these hurtful by-products have the potential to blend with water reservoirs/dams that can be utilized for drinking and by implication influence human wellbeing through the nourishment chain, reduce soil fertility and cause serious problems in their day-to-day activities [2-5]. In this manner, the treatment of these by-products is critical before they are discharge to the environ-

*Correspondence: Gashaw Beyene Kassahun (gashaw4nuclear@gmail.com)

Received: 15 August 2026; **Accepted:** 25 August 2026; **Published:** 15 September 2026

Copyright: © The Author(s), 2026. Published by Science Publishing Group. This is an **Open Access** article, distributed under the terms of the Creative Commons Attribution 4.0 License (http://creativecommons.org/licenses/by/4.0/), which permits unrestricted use, distribution and reproduction in any medium, provided the original work is properly cited.

ment/community. As a result, the treatment of these by-products is basic some time recently they are discharge to the environment/community. The degradation of such squander by-products, photocatalytic debasement strategy could be a promising method. Nowadays, nanotechnology and nanoscience have given extraordinary consideration for the synthesizing of alluring nano-materials with large ratio of surface to volume, one of a kind surface functionalities, and moo band-gap energy to treat industrial pollutants through oxidation processes. From one of progressed oxidation process methods, photocatalytic degradation technique is the effective means of cleaning up organic wastes [6]. In this technique, hydroxyl radicals are used to break down pollutants into safe minerals [2].

Polymeric semiconductors such as graphitic carbon nitride (g-C_3N_4) and polyaniline have garnered considerable interest in catalysis due to their non-toxic nature, low cost, abundance, ease of preparation, excellent thermal and chemical stability, unique layered structures, strong reducing capabilities, and highly adjustable band gap energies [7-10]. Due to the strong interface interaction, they are accelerating the transfer of photo-generated charges and they used as interchangeable. Graphitic carbon nitride is sustainable photocatalysts and prominent materials for the transformative of solution to energy crisis and environmental protection [11].

To address water pollution in Ethiopia, the authors have fabricated a novel material, namely a bismuth oxyhalide (BiOX, where X = Cl or Br)-based nanocomposite, which shows promise for this application. Due to their favorable physicochemical properties and excellent photocatalytic activity, bismuth oxyhalide-based materials are considered promising candidates for water purification. Based on these advantages, we fabricated $Bi_{12}O_{15}X_3$ (X = Cl or Br) heterojunctions with graphitic carbon nitride (g-C_3N_4). To the best of our knowledge, the present work reports, for the first time, the photocatalytic application of bismuth oxyhalide-based nanocomposites for the degradation of pollutants in water.

2. Materials and Methods

BiOX-based nanocomposites can be synthesized using various synthesis routes, such as thermal decomposition, hydrothermal synthesis, co-precipitation, polymerization, and solid-state reactions. The synthesized materials are characterized using X-ray diffraction (XRD) spectroscopy to investigate their crystal structure, crystallite size, phase composition, and lattice parameters; scanning electron microscopy (SEM) to examine their morphology, structure, and particle distribution; and UV–Vis spectroscopy to evaluate their optical properties. Finally, the photocatalytic performance of the synthesized materials is evaluated using different organic dyes as model pollutants, particularly methylene blue (MB) and methyl orange (MO), as well as real wastewater collected directly from the KK Textile Industry.

2.1. Materials

The precursors and solvents used to synthesize BiOX-based nanocomposites and evaluate their photocatalytic performance include bismuth nitrate pentahydrate ($Bi(NO_3)_3\ 5H_2O$), acetic acid, urea, ethylene glycol (EG), alcohol, deionized (DI) water, potassium chloride (KCl), potassium iodide (KI), potassium bromide (KBr), hydrochloric acid (HCl), and sodium hydroxide (NaOH). Methylene blue (MB) and methyl orange (MO) are used as model pollutants to evaluate the photocatalytic response. In addition, real wastewater, such as wastewater collected from a textile factory in Addis Ababa, is used to assess the practical applicability of the synthesized BiOX-based nanocomposites.

2.2. Methods

2.2.1. Photocatalytic Measurement

The photocatalytic performance of all synthesized samples will be evaluated using different dyes, namely methyl orange (MO) and methylene blue (MB), as model pollutants, as well as real wastewater collected from KK Textile Industry in Addis Ababa, Ethiopia. Briefly, 30 mg of the synthesized photocatalyst will be added to 30 mL of dye solution (10 mg/L) or an equivalent volume of contaminated wastewater. The suspension will then be magnetically stirred in the dark for 30 min to establish adsorption–desorption equilibrium. Since the photocatalytic efficiency is influenced by the concentrations of both the photocatalyst and the pollutant, the effects of these parameters will be investigated by varying their concentrations systematically. Subsequently, the suspension will be transferred to a photoreactor equipped with a circulating water system to minimize thermal effects caused by light irradiation. At predetermined irradiation intervals, 2 mL of the suspension will be withdrawn from the photoreactor. The collected samples will be centrifuged at 7000 rpm to remove the photocatalyst particles. Finally, the residual concentration of the dye or pollutants in the wastewater will be determined by measuring the absorbance at the corresponding maximum absorption wavelength (λ_{max}) using a UV–Vis spectrophotometer.

The photo-degradation efficiency (PDE) of the dyes and polluted water is calculated by applying the following equation.

$$PDE(\%) = \frac{C_0 - C}{C_0} \times 100 \quad (1)$$

The degradation data can be analyzed using the pseudo-first-order kinetic equation, $\ln(C_0/C_t) = kt$, which excludes the adsorption effect. Here, C_0 and C_t represent the solution concentrations at 0 minutes and at time t, respectively, and k is the pseudo-first-order rate constant (min^{-1}) [8, 12].

2.2.2. Synthesis of BiOX (X = Cl, Br)

BiOCl nanostructures were prepared by dissolving 2 mmol

of $Bi(NO_3)_3$ $5H_2O$ in 25 mL of ethylene glycol (EG) under continuous stirring for 20 min, following the method reported by Liu et al. (2019) [13]. Subsequently, 5 mL of 2 mmol KCl solution was added to the above solution, and the resulting mixture was vigorously stirred at room temperature for 60 min. The solution was then transferred to a Teflon-lined stainless-steel autoclave and subjected to hydrothermal treatment at 160 ℃ for 3 h. After cooling to room temperature, the resulting white precipitate was collected by centrifugation, washed several times with deionized water and ethanol, and dried at 80 ℃ for 24 h.

BiOBr nanostructures were synthesized using a similar procedure. However, 3.2 mmol of KBr was used as the bromide source instead of KCl, while the other synthesis conditions were kept unchanged.

2.2.3. Preparation of g-C_3N_4

Graphitic carbon nitride (g-C_3N_4) was synthesized using a facile calcination method. In this experiment, 10 g of urea powder (NH_2CONH_2) was accurately weighed and placed in an aluminum foil-lined crucible, which was then covered with a lid. The crucible containing the urea was placed in a muffle furnace and heated to 550 ℃ at a heating rate of 15 ℃/min. The temperature was maintained at 550 ℃ for 3 h. After calcination, the crucible was allowed to cool naturally to room temperature inside the furnace. The resulting product was then finely ground using a mortar and pestle. The obtained yellow powder was denoted as g-C_3N_4 and used for further characterization and experiments.

2.2.4. Synthesize of g-C_3N_4 @$Bi_{12}O_{15}Cl_3$ and g-C_3N_4 @$Bi_{12}O_{15}Br_3$

The g-C_3N_4@$Bi_{12}O_{15}Cl_3$ nanocomposite was synthesized by dissolving 5 g of $Bi(NO_3)_3$ $5H_2O$ in 50 mL of ethylene glycol (EG) under magnetic stirring at approximately 100 ℃ until a clear solution was obtained. Subsequently, 0.2 g of ultrathin g-C_3N_4, prepared as described in Section c (above), was added dropwise to the solution under continuous stirring for 10 min. The resulting precipitate was collected by centrifugation, washed several times with deionized water and ethanol, and dried at 70 ℃ for 20 h. The same procedure was followed to synthesize g-C_3N_4@$Bi_{12}O_{15}Cl_3$ using 0.3 g of g-C_3N_4.

3. Result and Discussion

3.1. XRD Result Analysis

XRD Result of g-C3N4@Bi12O15X3 (X = Br, Cl)

The XRD pattern of the pristine g-C_3N_4 sample exhibits two characteristic diffraction peaks at 2θ values of approximately 13.34 °and 27.38 °, which can be indexed to the (100) and (002) crystallographic planes [14], respectively. The weak peak at 13.34 ° is attributed to the in-plane structural ordering of the tri-s-triazine/heptazine units, corresponding to the (100) plane. In contrast, the strong diffraction peak at 27.38 ° is associated with the (002) plane, which originates from the interlayer stacking of the conjugated aromatic carbon nitride sheets. The high intensity of the (002) peak indicates a relatively well-ordered layered structure of g-C_3N_4.

The XRD patterns of $Bi_{12}O_{15}X_3$ (X = Cl or Br) exhibit several sharp and intense diffraction peaks, indicating the formation of a crystalline bismuth oxyhalide phase (similarly reported by [15-17]). The presence of well-defined and narrow diffraction peaks suggests a relatively high degree of crystallinity and good structural ordering of the synthesized $Bi_{12}O_{15}X_3$ materials. The positions and relative intensities of these diffraction peaks can be compared with the corresponding standard reference patterns to confirm the phase composition and crystal structure.

For the g-C_3N_4@$Bi_{12}O_{15}X_3$ heterostructures, the characteristic diffraction peaks of $Bi_{12}O_{15}X_3$ remain clearly visible, confirming that the crystalline structure of the bismuth oxyhalide is retained after composite formation. In addition, the characteristic diffraction peaks of g-C_3N_4 are observed around 13 °and 27–28 °, although their intensities are relatively weak compared with those of $Bi_{12}O_{15}X_3$. This reduction in intensity can be attributed to the low loading and/or high dispersion of g-C_3N_4 within the $Bi_{12}O_{15}X_3$ matrix, which makes its diffraction contribution less pronounced.

The appearance of the characteristic peaks of both g-C_3N_4 and $Bi_{12}O_{15}X_3$ in the composite provides evidence for the successful formation of the g-C_3N_4/$Bi_{12}O_{15}X_3$ heterostructure, rather than the formation of a completely new crystalline phase. A slight shift of the g-C_3N_4 (002) peak from approximately 27.38 °to 27.65 °toward a higher diffraction angle is also observed after composite formation. According to *Bragg's law*, $n\lambda=2d\sin\theta$, an increase in the diffraction angle corresponds to a decrease in the interplanar spacing (d). Therefore, this small peak shift suggests a slight reduction in the interlayer distance of g-C_3N_4, possibly resulting from interfacial interactions between g-C_3N_4 and $Bi_{12}O_{15}X_3$ during heterojunction formation.

Overall, the XRD results demonstrate that the synthesized materials possess good crystallinity and that the characteristic structures of both components are preserved in the g-C_3N_4@$Bi_{12}O_{15}X_3$ heterostructures. The structural interaction between the two components may facilitate interfacial charge transfer, which is particularly important for improving the photocatalytic performance of the composite.

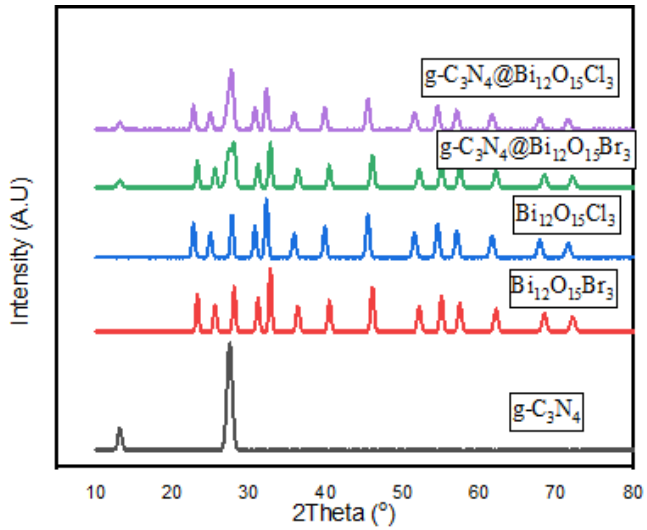

Figure 1. *XRD result of graphitic carbon nitride (g-C_3N_4), BiOBr, BiOCl, g-C_3N_4@$Bi_{12}O_{15}X_3$ (X = Br, Cl).*

3.2. SEM Image Analysis

3.2.1. SEM Image Analysis of BiOCl and BiOBr

As discussed in the previous section and related studies [18], the synthesized bismuth oxyhalide materials exhibit a nanosheet-like morphology. As shown in Figure 2, the SEM images confirm the formation of well-defined sheet-like structures for the synthesized $Bi_{12}O_{15}Cl_3$ and $Bi_{12}O_{15}Br_3$ samples.

The formation of a nanosheet-like morphology is particularly advantageous for photocatalytic applications because the large surface area and abundant exposed surface sites can provide more active sites for pollutant adsorption and photocatalytic reactions. Furthermore, the relatively thin morphology can shorten the diffusion distance of photogenerated charge carriers, which may reduce electron–hole recombination and facilitate charge separation. These characteristics make two-dimensional bismuth oxyhalide-based materials promising candidates for photocatalytic water purification and solar-energy-related applications. In the g-C_3N_4@$Bi_{12}O_{15}X_3$ composites, intimate contact between the nanosheet-like $Bi_{12}O_{15}X_3$ and g-C_3N_4 is also expected to promote interfacial charge transfer, thereby enhancing the photocatalytic performance of the heterojunction.

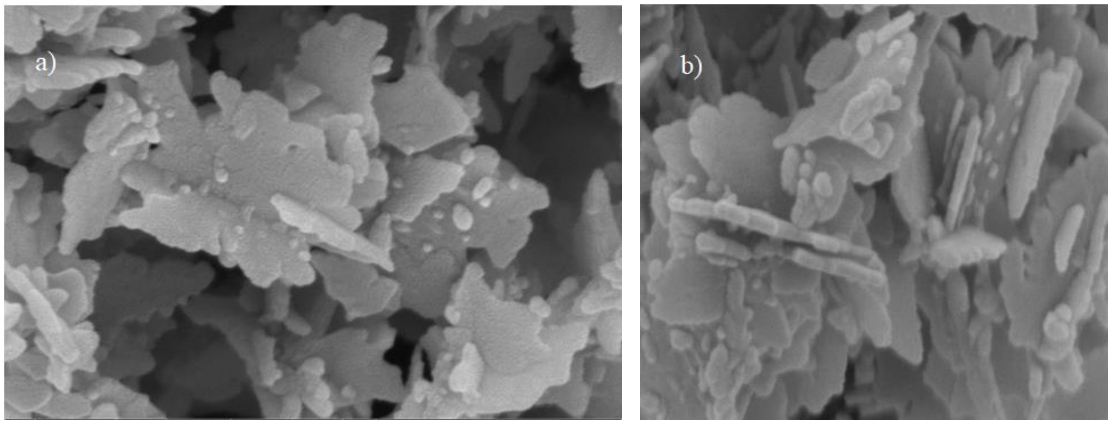

Figure 2. *SEM image of BiOCl (a) and BiOBr (b).*

3.2.2. SEM Image Analysis of $Bi_{12}O_{15}Cl_3$, $Bi_{12}O_{15}Br_3$, g-C_3N_4 @ $Bi_{12}O_{15}Cl_3$ and g-C_3N_4 @ $Bi_{12}O_{15}Br_3$

As shown by the SEM results, both the individual components and the resulting heterostructures exhibit a sheet-like morphology. However, after the formation of the composite, some morphological changes can be observed, which may be attributed to the interfacial interaction and rearrangement of atoms between the constituent materials. The close contact between the nanosheet-like structures may facilitate interfacial interactions and improve the accessibility of active surface sites.

The sheet-like morphology is particularly advantageous for photocatalytic applications because it can provide a large specific surface area, abundant active sites, and short charge-carrier diffusion pathways. Moreover, the two-dimensional structure can enhance the interaction between the photocatalyst surface and incident light, potentially improving light utilization. Therefore, the observed sheet-like morphology of the synthesized materials is expected to contribute positively to their photocatalytic performance. However, light absorption is also strongly dependent on the material's electronic and optical properties; therefore, the UV–Vis absorption results should be considered together with the SEM morphology to fully evaluate its light-harvesting capability.

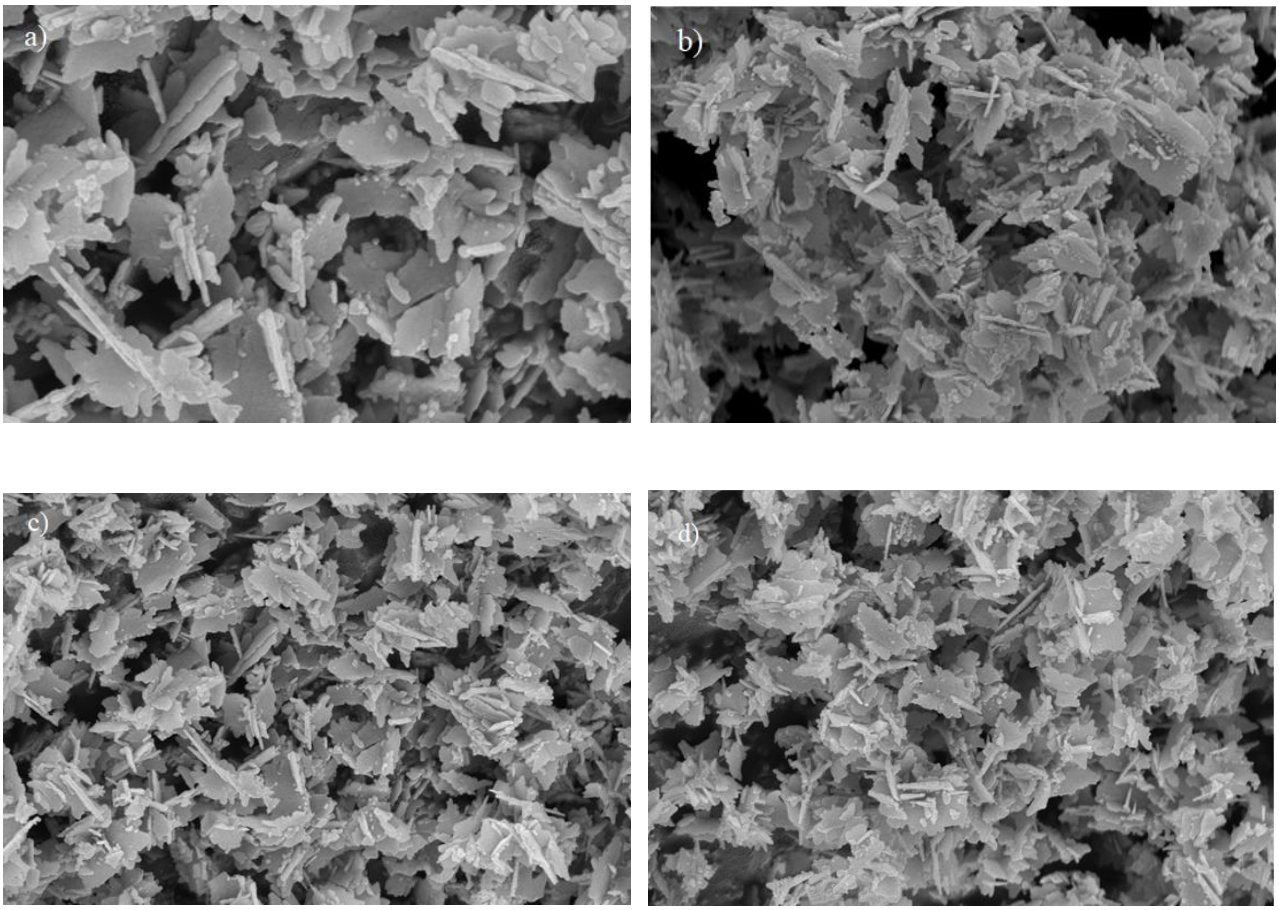

Figure 3. *SEM image of $Bi_{12}O_{15}Cl_3$ (a), $Bi_{12}O_{15}Cl_3$ (b), g-C_3N_4 @ $Bi_{12}O_{15}Cl_3$ (c) and g-C_3N_4 @ $Bi_{12}O_{15}Br_3$(d).*

3.3. UV-Vis Spectroscopy Analysis

3.3.1. UV-Vis Spectroscopy Analysis of g-C_3N_4@$Bi_{12}O_{15}X_3$ (X = Br, Cl)

The optical absorption properties of the synthesized materials were investigated using UV–Vis spectroscopy. The UV–Vis absorption spectra provide information about the light-absorption behavior of the materials and allow their optical band gap energies to be estimated. As shown by the absorption spectra, the absorption edges of the composite materials are shifted toward longer wavelengths compared with those of the individual components. In particular, the g-C_3N_4@$Bi_{12}O_{15}X_3$ heterostructures exhibit a pronounced red shift in their absorption edges, indicating an extended light-absorption range in the visible region. This enhanced visible-light absorption is beneficial for photocatalytic applications because it enables the materials to utilize a larger fraction of the incident solar spectrum.

The optical band gap energies of the synthesized materials were estimated from their corresponding absorption-edge plots. The estimated band gap energies of BiOCl, $Bi_{12}O_{15}Br_3$, $Bi_{12}O_{15}Cl_3$, g-C_3N_4@$Bi_{12}O_{15}Cl_3$, and g-C_3N_4@$Bi_{12}O_{15}Br_3$ were approximately 3.31, 2.92, 2.61, 2.48, and 2.36 eV, respectively. The progressive reduction in band gap energy after heterostructure formation suggests improved optical response and enhanced utilization of visible light.

The g-C_3N_4@$Bi_{12}O_{15}Br_3$ composite exhibits a lower band gap energy (2.36 eV) than g-C_3N_4@$Bi_{12}O_{15}Cl_3$ (2.48 eV). This difference can be attributed to the different electronic structures and interfacial interactions associated with Br- and Cl-containing bismuth oxyhalides. The formation of an intimate heterojunction between g-C_3N_4 and $Bi_{12}O_{15}X_3$ can modify the electronic structure and facilitate interfacial charge transfer, contributing to the observed reduction in the apparent optical band gap.

The band gap energy is an important parameter in photocatalysis because it determines the minimum photon energy required to excite electrons from the valence band to the conduction band. A narrower band gap generally allows a photocatalyst to absorb lower-energy photons and utilize a broader portion of visible light. Therefore, the reduced band gap and enhanced visible-light absorption observed for the g-C_3N_4@$Bi_{12}O_{15}X_3$ heterostructures, particularly g-C_3N_4@$Bi_{12}O_{15}Br_3$, are expected to contribute to improved photocatalytic activity. However, photocatalytic performance is also governed by factors such as charge separation, carrier lifetime, surface area, and surface reaction kinetics, not by band gap energy alone.

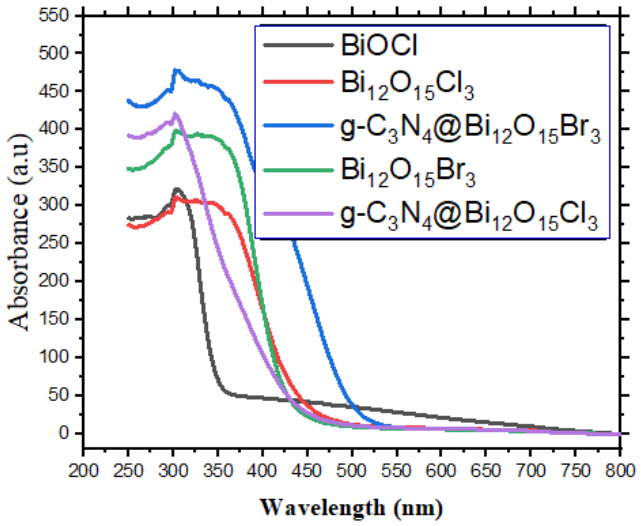

Figure 4. *Optical absorbance of BiOX and g-C_3N_4@$Bi_{12}O_{15}X_3$ based nano-composite.*

3.3.2. Photocatalytic Response

When the sample is exposed to light, the photocatalyst becomes excited, generating electron–hole pairs. The adsorbed oxygen particles on the photocatalyst interact with these electrons to produce superoxide anion radicals ($\bullet O_2^-$). Meanwhile, the surface hydroxyl groups react with the holes in the valence band, forming highly reactive hydroxyl radicals ($\bullet OH$). Both the hydroxyl ($\bullet OH$) and superoxide ($\bullet O_2^-$) radicals then attack the dye fragments adsorbed on the surface of photocatalyst, resulting in their photocatalytic degradation. The overall mechanism is illustrated schematically in Figure 5, with the corresponding reactions summarized below [7]:

1) $sample + hv \rightarrow e^-(CB) + h^+(VB)$
2) $e^- + O_2 \rightarrow \bullet O_2^-$
3) $h^+ + OH^- \rightarrow \bullet OH$
4) $\bullet OH + polutant \rightarrow degradation\ \ product$
5) $\bullet O_2^- + polutant \rightarrow degradation\ \ product$

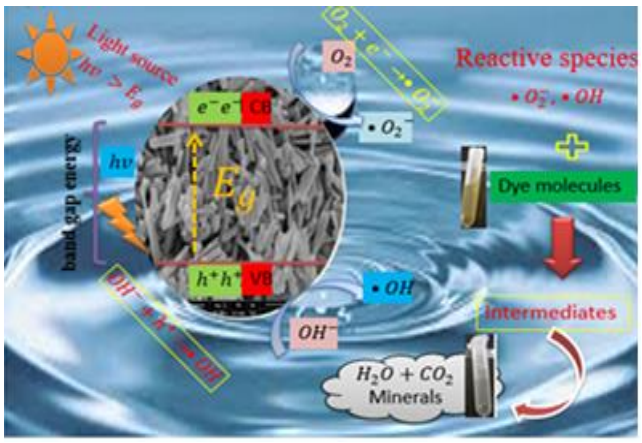

Figure 5. *Schematic mechanism of degradation of sample under light irradiation.*

The photocatalytic performance of prepared sample is depending on the morphology, size and shape intrinsic defects as well as method of preparation.

Photocatalytic Response of g-C_3N_4@$Bi_{12}O_{15}X_3$ (X = Cl, Br)

The photocatalytic performance of the g-C_3N_4@$Bi_{12}O_{15}X_3$ nanocomposites was evaluated under visible-light irradiation for 100 min. To assess their photocatalytic efficiency, different pollutants were used as model contaminants. As shown in Figure 6, both photocatalysts effectively degraded the selected dyes within the specified irradiation time. However, the percentage degradation obtained using the polluted water collected from KK Textile Industry, Addis Ababa, was lower than that obtained for the individual dye solutions. This lower degradation efficiency may be attributed to the presence of various organic and inorganic substances in the real wastewater, which can compete for active sites, absorb incident light, or interfere with the photocatalytic reaction.

As shown in the fourth panel of Figure 6, the degradation efficiencies of the three samples were compared at different irradiation times. Here, gBOC = g-C_3N_4@$Bi_{12}O_{15}Cl_3$, gBOB = g-C_3N_4@$Bi_{12}O_{15}Br_3$, and gBOB-K = g-C_3N_4@$Bi_{12}O_{15}Br_3$ tested using wastewater collected from KK Textile Industry. The results indicate that the degradation efficiencies of the photocatalysts increase with increasing irradiation time and show comparable photocatalytic behavior under the same experimental conditions.

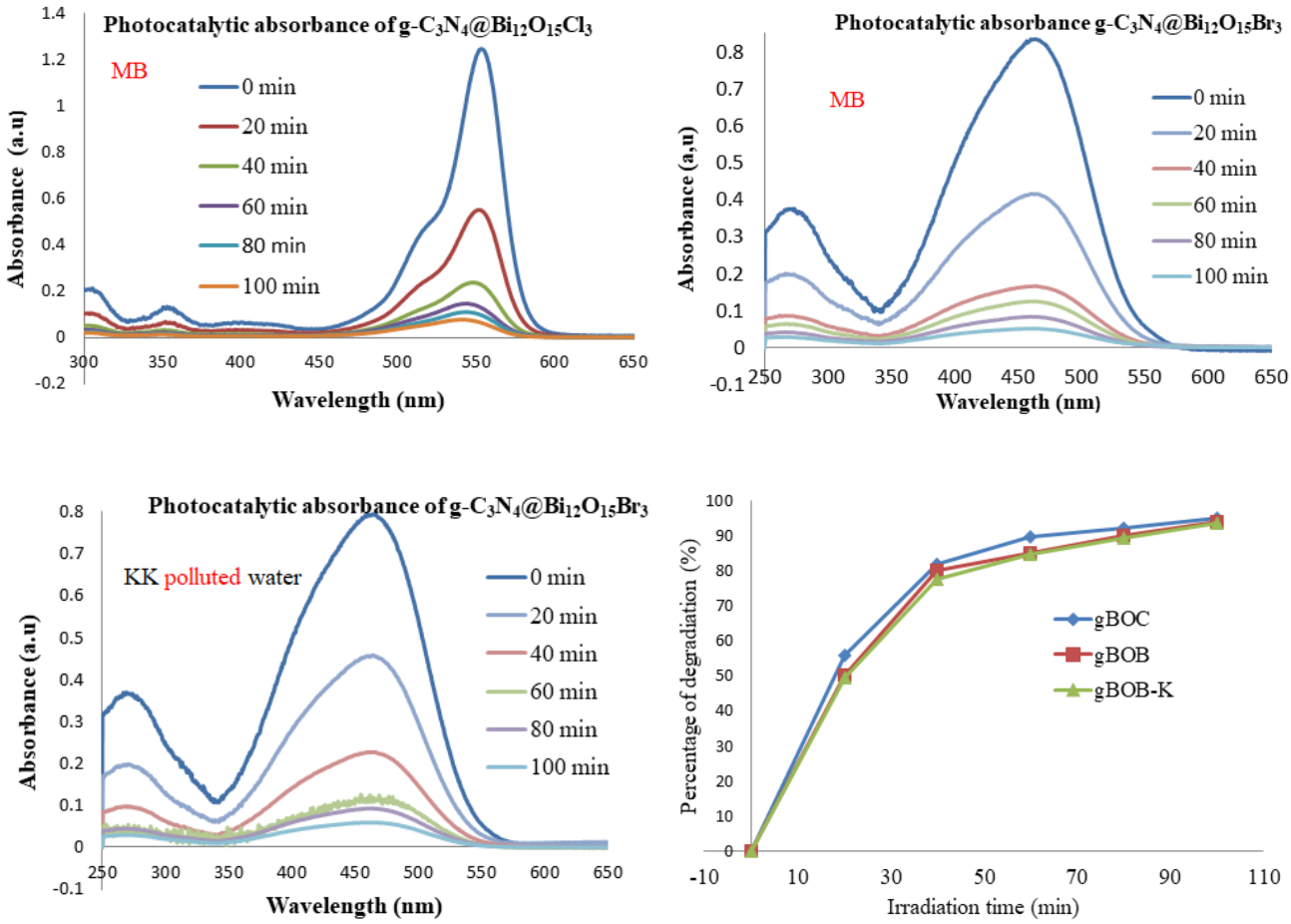

Figure 6. Photocatalytic response of g-C3N4@Bi12O15X3 material for different dyes.

Table 1. Percentage of degradation and photacatalytic activity of g-C_3N_4@$Bi_{12}O_{15}X_3$.

Sample	Dye	Irradiation time (min)	Degradation (%)	Photacatalytic activity 10^{-3} (min^{-1})
g-C_3N_4@$Bi_{12}O_{15}Cl_3$	MB	100	97.95	29.9
g-C_3N_4@$Bi_{12}O_{15}Br_3$	MB	100	96.97	27.2
g-C_3N_4@$Bi_{12}O_{15}Br_3$	KK polluted water	100	96.76	27

3.3.4. Cyclic Stability of g-C_3N_4@$Bi_{12}O_{15}Cl_3$

From an economic and environmental perspective, the reusability of synthesized photocatalytic materials is of great importance in the field of catalysis [6]. In this study, the cyclic stability of the as-prepared g-C_3N_4@$Bi_{12}O_{15}Cl_3$ photocatalyst was evaluated over four consecutive catalytic cycles using methylene blue (MB) as a model pollutant.

As illustrated in Figure 7, the recycled photocatalyst exhibited no significant loss in photodegradation efficiency even after four consecutive cycles, indicating its good chemical stability and resistance to photocorrosion during the degradation of the model pollutant. The results demonstrate that the g-C_3N_4@$Bi_{12}O_{15}Cl_3$ nanocomposite possesses good photocatalytic stability and reusability. Therefore, the g-C_3N_4@$Bi_{12}O_{15}X_3$ (X = Cl, Br) heterostructures show promising potential for repeated use in practical photocatalytic applications, particularly in wastewater treatment.

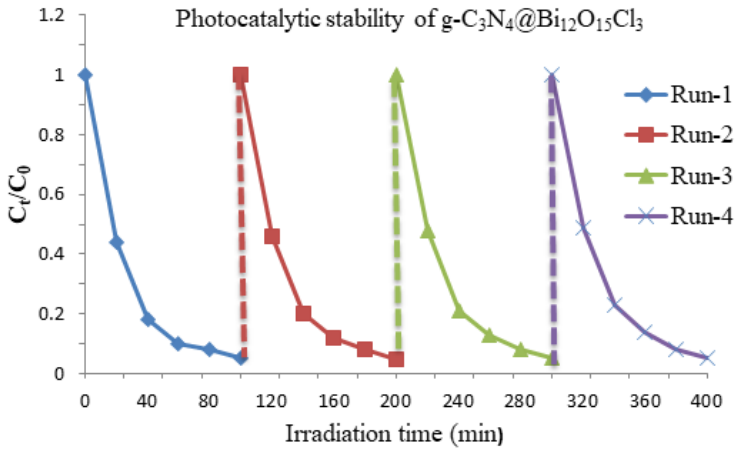

Figure 7. *Cyclic photodegradation curve for the composite g-C_3N_4@$Bi_{12}O_{15}Cl_3$ photocatalyst.*

4. Summary

Bismuth oxyhalide (BiOX)-based nanocomposites possess several attractive physicochemical and optical properties, including suitable band gap energies, strong visible-light absorption, high chemical stability, and favorable charge-transfer characteristics. These properties make BiOX-based materials promising candidates for a wide range of applications, particularly in photocatalytic water treatment, solar-energy conversion, and other environmental remediation processes. However, the photocatalytic performance of pristine BiOX materials can be further improved by modifying their structural, optical, and electronic properties. In this regard, several strategies, including doping, heterostructure formation, and modification of the chemical composition of BiOX, can be employed to enhance their performance.

In the present research project, g-C_3N_4@$Bi_{12}O_{15}X_3$ (X = Cl and Br) nanocomposites were synthesized through appropriate synthesis routes, and their structural, morphological, and optical properties were investigated using different characterization techniques. The formation of the heterostructures was confirmed through complementary characterization methods, including X-ray diffraction (XRD), scanning electron microscopy (SEM), and UV–Vis spectroscopy. The results demonstrated that the synthesized materials possess well-defined crystalline structures, sheet-like morphologies, and improved optical absorption characteristics compared with the individual components.

The photocatalytic performance of the synthesized nanocomposites was also systematically evaluated using methylene blue (MB) and methyl orange (MO) as model pollutants, as well as real wastewater collected from a textile industry. The synthesized photocatalysts demonstrated excellent photocatalytic activity under visible-light irradiation. The degradation efficiencies of the investigated materials exceeded 96.5% for both the model pollutant solutions and real wastewater under the employed experimental conditions. These results indicate that the formation of a g-C_3N_4/$Bi_{12}O_{15}X_3$ heterojunction can effectively improve the light-harvesting capability and facilitate the separation and transfer of photogenerated charge carriers, thereby enhancing photocatalytic degradation.

In addition to photocatalytic activity, the reusability and stability of the synthesized photocatalysts were investigated through repeated degradation cycles. The photocatalytic materials maintained their degradation performance after four consecutive cycles, with no significant decrease in activity. This result indicates that the synthesized heterostructures possess good structural stability and resistance to photocorrosion during the photocatalytic process.

Overall, the findings of this research demonstrate that g-C_3N_4@$Bi_{12}O_{15}X_3$ (X = Cl, Br) nanocomposites are promising visible-light-responsive photocatalysts for the degradation of organic pollutants. Their high photocatalytic efficiency, good stability, and reusability suggest that these materials have considerable potential for practical wastewater treatment and environmental remediation applications. Further optimization of the composition, interfacial structure, and synthesis conditions could potentially improve their performance and facilitate their application on a larger scale.

Abbreviations

MB	Methylene Blue
MO	Methyl Orange
XRD	X-ray Diffraction
SEM	Scanning Electron Microscopy
UV-Vis	Ultra Violet Visible
PDE	Photo Degradation Efficiency

Author Contributions

Gashaw Beyene: Conceptualization, Investigation, Writing – original draft

Kinde Yeneayehu: Investigation, Writing – review & editing

Conflicts of Interest

The authors declare no conflicts of interest.

References

[1] Yohannes. H. (2017)., Elias E, Contamination of Rivers and Water Reservoirs in and Around Addis Ababa City and Actions to Combat It. *Environ Pollut Climate Change*, 116.

[2] Taghvaei H, F. M. (2018). Preparation, characterization and photocatalytic degradation of methylene blue by Fe^{3+} doped TiO_2 supported on natural zeolite using response surface methodology. *Adv Environmetal Technol*, 205-216.

[3] Sethi D, (2017). ZnO/TiO2 composites for photocatalytic inactivation of Escherichia coli. *J Photochem Photobiol B Bio*, 168, 117-123, https://doi.org/10.1016/j.jphotobiol.2017.02.005

[4] Zhuang H, X. W. (2019). Construction of one dimensional ZnWO4@SnWO4 core-shell heterostructure for boosted photocatalytic performance. *J Mater Sci Technol*, 2312-2318, https://doi.org/10.1016/j.jmst.2019.05.036

[5] Yousefi H. (2019). Photocatalytic properties of Ag@Ag-doped ZnO core-shell nanocomposite. *J Photochem Photobiol A Chem*, 71-76, https://doi.org/10.1016/j.jphotochem.2019.02.008

[6] Dong P, (2015). Synthesis and photocatalytic activity of Ag_3PO_4/$TiOF_2$ composites with enhanced stability. *Mater Lett*, 143, 20-23 https://doi.org/10.1016/j.matlet.2014.12.063

[7] Beyene, G. et al, (2020). Rapid synthesis of triple-layered cylindrical ZnO@SiO_2@Ag core-shell nanostructures for photocatalytic applications. *J. Nanopart. Res.*, 355, https://doi.org/10.1007/s11051-020-05086-0

[8] Ni. Han. (2020). Qixiang Xu, Gashaw Beyene, Qinfang Zhang, Enhanced photocatalytic activity over g-C_3N_4/$(BiO)_2(OH)_xCl_{2-x}$ Z-scheme heterojunction. *Applied Surface Science*, 146464, https://doi.org/10.1016/j.apsusc.2020.146464

[9] Kumar. A. et. al. (2018). Quaternary magnetic BiOCl/g-C_3N_4/Cu_2O/Fe_3O_4 nano junction for visible light and solar powered degradation of sulfamethoxazole from aqueous environment. *Chemical Engineering Journal*, 462-478, https://doi.org/10.1016/j.cej.2017.10.049

[10] Liu. H. (2018). N-doped $CsTi_2NbO_7$@g-C_3N_4 core-shell nanobelts with enhanced visible light photocatalytic activity. *Materials Letters*, 235-238, https://doi.org/10.1016/j.matlet.2018.01.098

[11] Dhavalkuma. Bhanderi. (2024). Graphitic carbon nitride (g-C 3N 4) as an emerging photocatalyst for sustainable environmental applications: a comprehensive review. *RSC Sustanability*, 265-287, https://doi.org/10.1039/d3su00382e

[12] Vela-V ázquez. R. etal. (2015). Bismuth oxyiodide-oxychloride mixed phase nanocomposites: synthesis, adsorption capacity, and photocatalytic activity under visible light. *J Nanopart Res (2025)*, 26: 5, https://doi.org/10.1007/s11051-024-06194-x

[13] Liu. J. etal. (2019). Fabricating visible-light photoactive 3D flower-like BiOCl nanostructures via a one-step solution chemistry method at room temperature. *Applied surface science*, 247-252, https://doi.org/10.1016/j.apsusc.2019.02.102

[14] Zhenzong. Z. (2020). In-situ growth of all-solid Z-scheme heterojunction photocatalyst of Bi7O9I3/g-C3N4 and high efficient degradation of antibiotic under visible light. *Applied Catalysis B*, 118212, https://doi.org/10.1016/j.apcatb.2019.118212

[15] Soun Xu et al (2024), Efficient photocatalytic degradation of tetracycline using Z-scheme GCN/$Bi_{12}O_{17}Br_2$ composites under visible light: Process and mechanism, Colloids and Surfaces A: Physicochemical and Engineering, 682, 132903, https://doi.org/10.1016/j.colsurfa.2023.132903

[16] Wen et al. (2025), Recent advances on $Bi_{12}O_{17}Cl_2$-based photocatalysts for energy and environmental application. Journal of Cleaner Production, 495, 145060, https://doi.org/10.1016/j.jclepro.2025.145060

[17] Xue et al. (2025), MOF-derived $Bi_{12}O_{17}Br_2$/Bi_2O_3/$Bi_{25}FeO_{40}$ for efficient photocatalytic removal of bisphenol pollutants under visible light. Applied Surface Science, https://doi.org/10.1016/j.apsusc.2025.163431

[18] Puttaraju. T. etal. (2022). Synthesis of bismuth oxychloride nanoparticles via co-precipitation method: Evaluation of photocatalytic activity. *Materials Today: Proceedings*, 5533-5539, https://doi.org/10.1016/j.matpr.2022.04.333